

Article

Effects of the Heat Treatment in the Properties of Fibrous Aerogel Thermal Insulation

Ákos Lakatos ^{1,*}, Attila Csík ², Anton Trník ^{3,4} and István Budai ⁵

¹ Department of Building Services and Building Engineering, Faculty of Engineering, University of Debrecen, Ótemető str 2-4 1, 4028 Debrecen, Hungary

² Institute for Nuclear Research, Hungarian Academy of Sciences, Bem tér 18/c, 4026 Debrecen, Hungary; csik.attila@atomki.mta.hu

³ Department of Physics, Faculty of Natural Sciences, Constantine the Philosopher University in Nitra, Tr. A Hlinku 1, 94974 Nitra, Slovakia; atrnik@ukf.sk

⁴ Department of Materials Engineering and Chemistry, Faculty of Civil Engineering, Czech Technical University in Prague, Thákurova 7, 16629 Prague, Czech Republic

⁵ Department of Engineering Management and Enterprise, Faculty of Engineering, University of Debrecen, Ótemető str 2-4, 4028 Debrecen, Hungary; budai.istvan@eng.unideb.hu

* Correspondence: alakatos@eng.unideb.hu; Tel.: +36-3033-468-61

Received: 29 April 2019; Accepted: 22 May 2019; Published: 25 May 2019



Abstract: Nowadays, besides the use of conventional insulations (plastic foams and wool materials), aerogels are one of the most promising thermal insulation materials. As one of the lightest solid materials available today, aerogels are manufactured through the combination of a polymer with a solvent, forming a gel. For buildings, the fiber-reinforced types are mainly used. In this paper, the changes both in the thermal performance and the material structure of the aerogel blanket are followed after thermal annealing. The samples are put under isothermal heat treatments at 70 °C for weeks, as well as at higher temperatures (up to 210 °C) for one day. The changes in the sorption properties that result from the annealing are presented. Furthermore, the changes in the thermal conductivity are followed by a Holometrix Lambda heat flow meter. The changes in the structure and surface of the material due to the heat treatment are investigated by X-ray diffraction and with scanning electron microscopy. Besides, the above-mentioned measurement results of differential scanning calorimetry experiments are also presented. As a result of using equipment from different laboratories that support each other, we found that the samples go through structural changes after undergoing thermal annealing. We manifested that the aerogel granules separate down from the glass fibers and grow up. This phenomenon might be responsible for the change in the thermal conductivity of the samples.

Keywords: fibrous aerogel; thermal conductivity; heat treatment; XRD; SEM; DSC

1. Introduction

A method to decrease the energy use as well as the emission of greenhouse gases is to apply thermal insulation materials. [1–4] Silica aerogels are mesoporous materials that have very small thermal conductivity (λ , W/mK) [5]. Aerogel materials are applied as thermal excellent insulations. It has been presented in recent papers that fibrous, transparent, or translucent aerogel-type insulations are some of the most innovative/advanced insulation materials. Aerogel is a porous material with low density, and cells on the nanoscale. It is manufactured from different types of gels by supercritical drying; silica alco-gels are the most widely manufactured, which are most regularly prepared from silica gel [6–11]. In many papers, in the systematic literature, investigations of aerogel-related contents can be found, but due to a lack of space, only some of them can be presented as well as processed in the introduction part of this paper [12–14]. The main goal of this paper is to present and understand experimental

results carried out on glass fiber-reinforced aerogel samples. The thermo-hygric properties of the aerogel have been comprehensively presented in recent papers [15–20].

It was previously presented in [6] that through service time, the thermal conductivity of the samples varies. On the nanometric and microscopic scale, it strongly depends on the distribution and size of the fibers.

It should be stated that over a temperature interval ($-15\text{ }^{\circ}\text{C}$ to $25\text{ }^{\circ}\text{C}$), the effect of air temperature has a negligible or only minor influence on the thermal conductivity coefficient of a sample; nevertheless, at uncommon temperature varieties ($25\text{ }^{\circ}\text{C} < T < 200\text{ }^{\circ}\text{C}$), significant changes are expected. Near these mentioned temperatures, which can be thought to be thermal, annealing, materials can suffer physical or chemical changes and can also provoke a rise in thermal conductivity.

High temperature can raise the kinetic reaction rates inside the materials, and can probably boost the chemical, as well as the physical degradation phenomenon [21]. In industrial cases, higher (elevated) temperature impacts can reach the materials. By insulating pipes, transporting hot fluid or steam, or heating, ventilation, and air conditioning (HVAC) systems with temperatures of up to $200\text{ }^{\circ}\text{C}$ – $300\text{ }^{\circ}\text{C}$ can be formed.

The stable thermal resistance is a property that is required for formulating the design insulation performance under service conditions. Controlled aging is a method for modeling the chemical, mechanical, and thermal (physical) properties of a sample as a function of time. Whether thermal annealing causes elevated aging regarding the silica aerogel bats is unknown, so measurements and models are necessary. Having a relatively high melting point, general temperature ranges ($-10\text{ }^{\circ}\text{C}$ to $60\text{ }^{\circ}\text{C}$) would not have a substantial influence, but the higher temperatures would have. Jelle et al., in their paper, presented thermal exposures as aging issues, for example: the thermal annealing [21,22]. Miros revealed that heat annealing as a thermal aging procedure influenced the thermal properties of mineral wool materials at unconventional temperature ranges ($100\text{ }^{\circ}\text{C}$ to $600\text{ }^{\circ}\text{C}$) [23]. Furthermore, for insulation such as rock wools or fibrous silica aerogels, the deterioration of the thermal performance should appear through chemical or physical reactions as structural modifications. Similar to the paper of Miros [23], where aging caused structural changes followed by variations in the thermal conductivity. They explored changes with a heat flow meter.

In recent years, besides the measurements of the thermal conductivities and sorption isotherms under normal (general conditions), test results on heat-treated samples were presented as well. These ordinary measurements are usually completed with destructive or non-destructive structural investigations e.g., scanning electron microscopy, calorimetry, and diffraction for crystallization study. It has been well presented in previous papers [24,25] that scanning electron microscopy (SEM) combined with element mapping could illustrate essential information regarding the structures and orders of the fibers [26,27]. After annealing, an analysis of the microstructure of the samples is very important. Moreover, besides these investigations, tests with an X-ray diffractometer (XRD) should be carried out. Several papers [28,29] present the XRD measurements of the aerogels after annealing at elevated temperatures, which are usually over $500\text{ }^{\circ}\text{C}$. Also, differential scanning calorimetry (DSC) investigations combined with scanning electron microscopy as well as with sorption measurements were executed on aerogels [30,31].

In this study, we systematically investigated the influence of different aging and temperatures on the structure and thermal conductivity of glass fiber-enhanced silica aerogel, with 150 kg/m^3 density. Then, changes in the sorption isotherms as well as modification in the structure and in the thermal properties are introduced after executing SEM, DSC, and XRD tests. The samples applied in this study were received from a Hungarian distributor.

2. Materials and Methods

2.1. Thermal Conductivity Measurements

The measurement of the thermal conductivity of insulation materials can be performed by following the rules of the EN ISO 12664:2001 standard [32] (Thermal performance of building materials and products. Determination of thermal resistance by means of guarded hot plate and heat flow meter methods. Dry and moist products of medium and low thermal resistance) [24,29]. In order to reveal the exact thermal conductivity coefficient of our samples, a Holometrix Lambda 2000 type heat flow meter (HFM) (Bedford, Massachusetts, US) was applied. The used equipment was manufactured to specify the thermal conductivity coefficient of insulation materials with about 5% accuracy, which is in agreement with standards ASTM C518 [33] and ISO 8301 [34]. As the basis of the research, the thermal conductivity measurement results were presented in a previous paper [6] and here, these results will be improved through a deeper engineering analysis of the materials. The measurement conditions can be found in [6,18,35–37].

2.2. Sorption Isotherm Measurements

In order to find the moisture/vapor sorption properties of the samples, three pieces of equipment should be combined: a drying apparatus, a climatic chamber, and a milligram precision balancer. First, in order to find the sorped amount of water, the materials should be desiccated to a changeless weight, which in our case is a Venticell 111 apparatus (MMM Medcenter Facilities GmbH, München, Germany). It works with hot air between 10–250 °C. By using the equipment, the material can be dried; furthermore, samples can be thermally (heat) treated by setting different temperature values [6,18,35–37].

After treating the samples in this heater/dryer to constant mass, their weights must be registered with a balance. Afterwards, samples need to be positioned in a climatic chamber, which in our case is a Climacell 111 apparatus (MMM Medcenter Facilities GmbH, München, Germany). The apparatus can fix the temperature between 0–100 °C with any humidity between 10–90%.

For recording the sorption isotherms curves, four aerogel samples with 1-cm thickness and a 10 cm × 10 cm base area were tested. The investigations were done by following the rules of ISO 12571: 2013 standard [38] (Hygrothermal performance of building materials and products—Determination of hygroscopic sorption properties, Part B—climatic chamber method). In the humidity chamber, the temperature was fixed to 23 ± 1 °C, while the relative humidities were 30%, 50%, 65%, 80%, and 90%. From the wet and dry masses of all the samples, the moisture contents were calculated, and the results were averaged. The sorption isotherm of the unannealed sample was referred to in our previous work [6], while the graph for the two annealed samples is presented here.

2.3. Differential Scanning Calorimetry Measurements

The specific heat capacity (c_p) was determined according to standard DIN 51007 [39], where a differential scanning calorimetry (DSC) and a sapphire as the calibrant are used. DSC was carried out using a DSC 822e (Mettler Toledo, Greifensee, Switzerland) device. The experiments were done in the temperature interval from 25 °C up to 300 °C in an air atmosphere with a flow rate of 50 mL/min. The heating rate was 10 °C/min and the isothermal regime (5 min) was applied before and after linear heating. The mass of samples was about 9 mg, and aluminum crucibles (volume of 40 mm³) with lids were used.

The specific heat capacity was calculated from the measured heat flow data of empty crucibles, a sapphire, and a sample using the equation:

$$c_p = c_{pc}(m_c(A_s - A_b))/(m_s(A_c - A_b)) \quad (1)$$

where A_b , A_s , and A_c (in W/g) are the measured amplitudes (heat flows) of the empty crucibles, sample, and sapphire, respectively. Moreover, m_c and m_s (in g) are the masses of the sapphire and sample, respectively, and c_{pc} (in J/(kg·K)) is the specific heat capacity of the sapphire [34].

2.4. Heat Treatments of the Samples

The heat-treating of the samples was executed in the VentiCell 111 apparatus (MMM Medcenter Facilities GmbH, München, Germany), in which the samples can be heat treated or dried at different air temperatures ranging between 10–250 °C. The equipment works with air circulation using an inbuilt ventilator [6,18,35–37]. The measurements were performed according to the ISO 12664 [32] and 12667 [40] standards. The tests were executed before and after thermal annealing the samples. Two different thermal annealing rows were done. The samples were put under isothermal heat treatments at 70 °C for six weeks (isothermal heat treatment); they were also put under thermal treatment at higher temperatures (70 °C, 100 °C, 130 °C, 150 °C, 180 °C, and 210 °C) for one day on the same sample, one after the other.

2.5. X-ray Diffraction Experiments

Crystallographic information from the as-received and annealed samples has been obtained by applying the X-ray diffraction (XRD) method. The measurements were performed by a Siemens diffractometer (Kristalloflex 710H, Siemens, Karlsruhe, Germany) using $\text{CuK}\alpha$ irradiation with $\lambda = 0.154$ nm. Scanning geometry between θ – 2θ was applied to perform the measurements; the X-ray tube was operated with 40 mA and 40 kV settings. The high-angle spectra were measured between 20–85° to study the presence of solid phases in the samples.

2.6. Scanning Electron Microscopy Investigations

The materials were analyzed using a Hitachi TM-3030 scanning electron microscope (SEM) (Hitachi High-Technologies Europe GmbH, Japan) with a Bruker Quantax 70 EDS system (Berlin, Germany). The TM3030 is equipped with premium signal detectors that have been incorporated in field emission (FE-SEM) and variable-pressure (VP-SEM) and provide unparalleled image quality. The detectors can be effectively operated under low-vacuum conditions and can support high-sensitivity four-segment semiconductor (BSE) detector for image observation without metal coating. The TM-3030 can be used to observe BSE images with a magnification range from 15 to 30,000×. Element mapping (energy-dispersive spectroscopy, EDS) with X-ray analysis with a wide detection area (30 mm²) was executed on the samples as well.

3. Results

3.1. Thermal Conductivity Results

In a recent paper [6], it was presented that the thermal conductivity remains constant after annealing the samples until 42 days under atmospheric pressure and at 70 °C. It was found that the thermal conductivity ranges around 0.017 W/(m·K). This thermal conductivity value was equal to that measured on the as-received (unannealed) sample. However, after annealing the samples at 100 °C, 150 °C, 180 °C, and 210 °C for one day (one after the other on the same sample), the thermal conductivity was changed. Between 100–200 °C, it changes up to 0.018 W/(m·K), while above 200 °C, it jumps up to 0.020 W/(m·K) [6]. In order to go deeper into the reasons of the changes, further experiments were executed.

3.2. Results of Sorption Isotherm Measurements

Sorption isotherm investigations were executed with the above-mentioned method. In Figure 1, the sorption isotherm curves (equilibrium moisture content versus relative humidity at 23 °C) of annealed samples at 70 °C for 42 days and the graph of the thermally treated sample at 100 °C, 150 °C, 180 °C, and 210 °C for one day are visible. The sorption isotherm of the unannealed samples was also presented in [6]. The shape of the sorption isotherm of the as-received sample shows continuously

increasing moisture content with the increasing relative humidity, and without any breaks in it. This shape presents the type II isotherm of the new classification of the BET isotherm representing adsorption isotherms on macroporous adsorbents with strong affinities [41].

Interestingly, one can see that the shapes of the sorption isotherms of the annealed samples are different. Between 50–75% relative humidity, the isotherms have a strong break. After analyzing the shape of the sorption isotherms, one can state that these shapes can be identified as type-IV isotherms, which characterizes mesoporous adsorbents with strong affinities [41]. We should conclude here that some structural change occurred due to the thermal annealing.

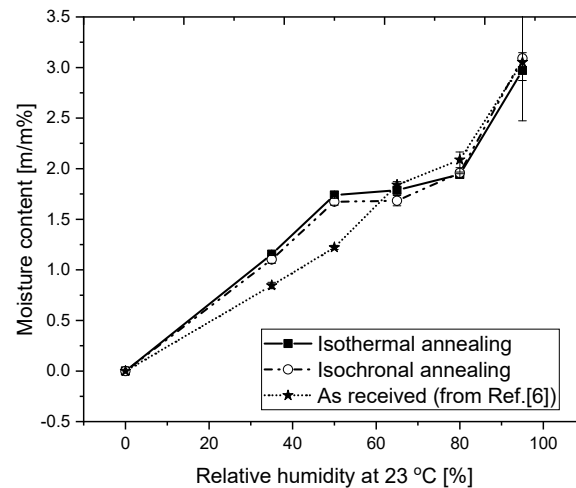


Figure 1. The sorption isotherm graphs.

3.3. Scanning Electron Microscope Results

To visualize the expected changes in the structures, scanning electron microscope measurements were executed. Pieces of unannealed, isothermally annealed, and isochronally annealed samples were put under an SEM test into the microscope. The results are presented in Figures 2–5 as: (Figure 2) an SEM image of the as-received sample, (Figure 3) an EDS element map of the as-received sample, (Figure 4) an SEM image of the isothermally annealed sample, and (Figure 5) an SEM image of the isochronally annealed sample. From the SEM pictures (Figure 2), it can be seen that the aerogel granules are joined to the fibers, which is in good connection with the other images presented in the literature [24,26].



Figure 2. SEM image of the as-received sample.

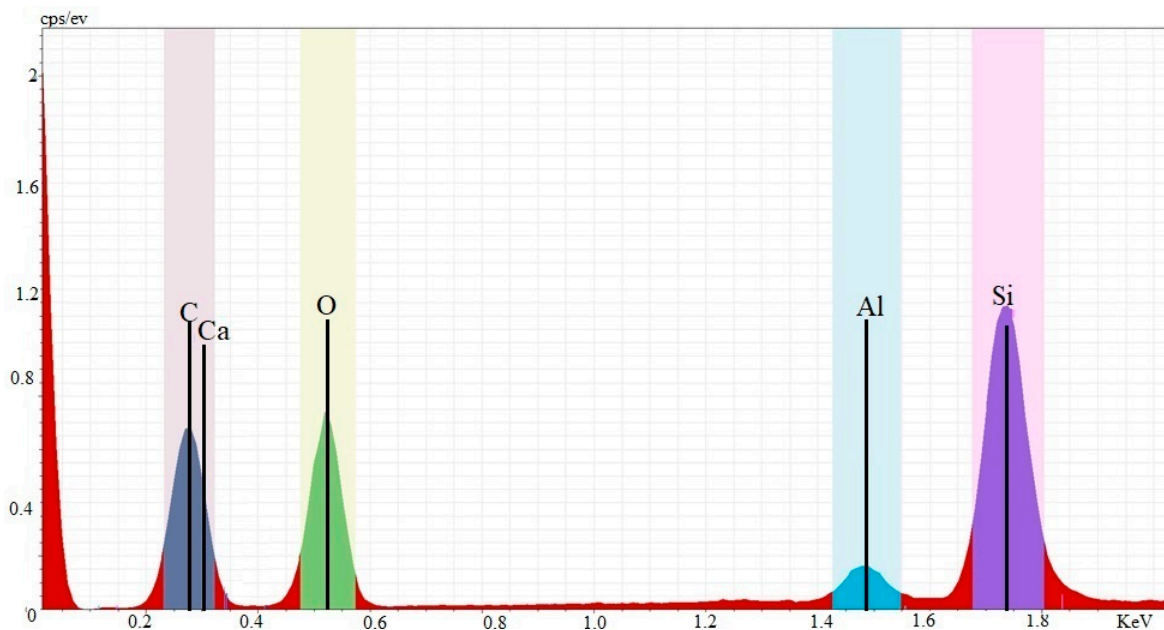


Figure 3. Energy-dispersive spectroscopy (EDS) element map of the as-received sample.

From the element maps, one can observe that the main components of the sample—silicon, oxygen, aluminum, and some calcium and carbon contaminants—may be coming from the glass fibers.

From the obtained SEM images, we can conclude that the particles after annealing are separated from the fibers and create bigger granulates. It can be clearly stated that the structure of the samples is changing due to the heat treatment. After thermal annealing at high temperatures, one cannot observe any particles on the fibers, while aerogel particles are visible on the surface of the fibers of the as-received and isothermally annealed samples. A similar effect was predicted by Li et al. and Yang et al. [24,26]. Iswar et al. visualized similar effects with SEM after annealing the samples at 65 °C from 2 h to 24 h [5]. Liang et al. [42] postulated that the investigations of the service life of aerogel-based insulations can be achieved by scanning electron microscope, too.

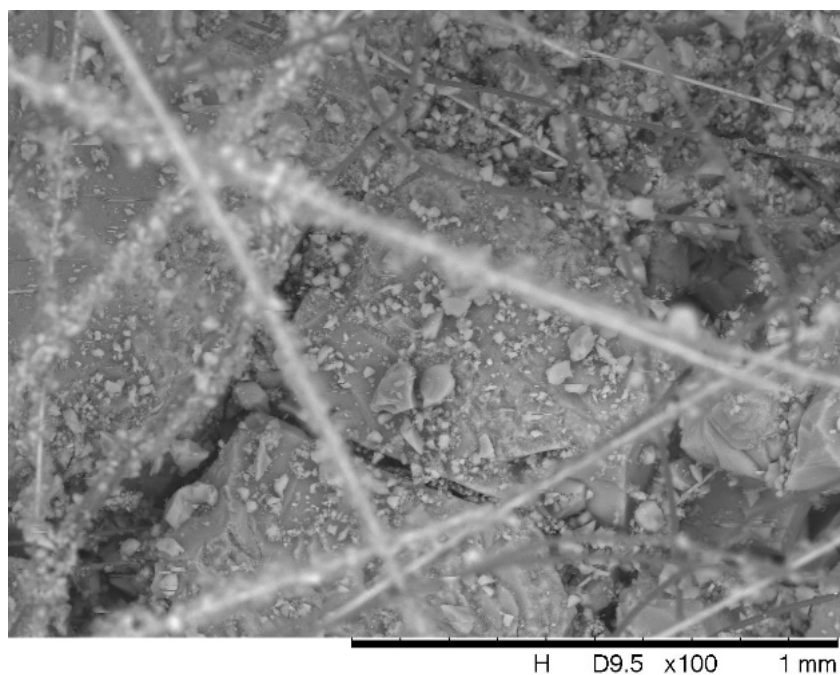


Figure 4. SEM image of the isothermally annealed sample.

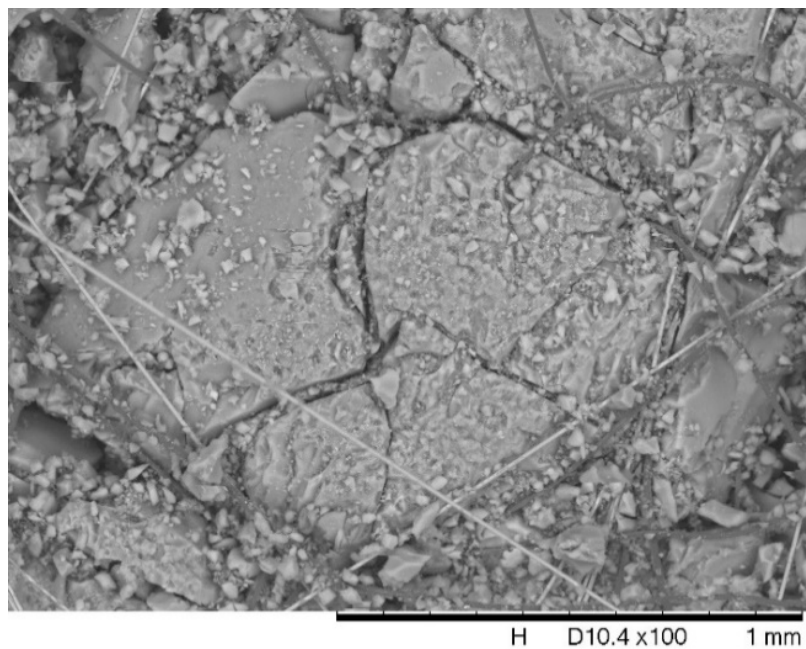


Figure 5. SEM image of the isochronally annealed sample.

3.4. Differential Scanning Calorimetry Results

Figure 6 shows the DSC results of an as-received sample.

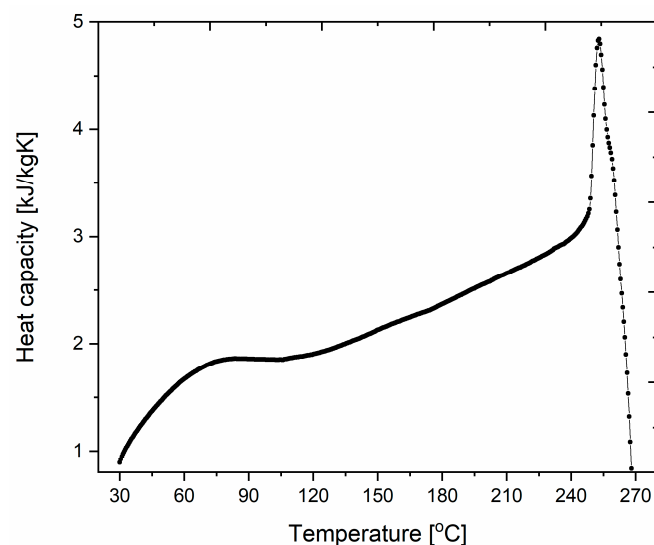


Figure 6. The differential scanning calorimetry (DSC) results of the aerogel sample.

From Figure 6, it is visible that the specific heat capacity at room temperature is about 1000 J/(kg·K), while it is constant almost between 70–120 °C. After this, a continuously increasing part is visible, while a great change is observable above 240 °C. Here, some reaction might take place. Hasan et al. [30] presented combined measurements on aerogel samples, including calorimetry tests. They showed a critical region between 130–260 °C.

3.5. Results of XRD Measurements

In order to further investigate our samples and check structural changes, XRD measurements were performed on all three types of samples. As it was already presented in [28,29,43,44], XRD is reasonable tool to understand the structural form of the aerogel samples. The results are presented in

Figures 7–9 as: (Figure 7) XRD spectra of the as-received sample, (Figure 8) the XRD spectra of the isothermally annealed samples, and (Figure 9) the XRD spectra of the isochronally annealed samples. Zhu et al., Kwon and Choi, and Music et al. [29,43,44] show the characteristic peak near 22–23° that belong to the amorphous SiO₂ phase. Additionally, Zhu et al. [28] further observed a small peak near 43° as it is also visible in our results (Figure 7), where the XRD spectra of the as-received sample are presented.

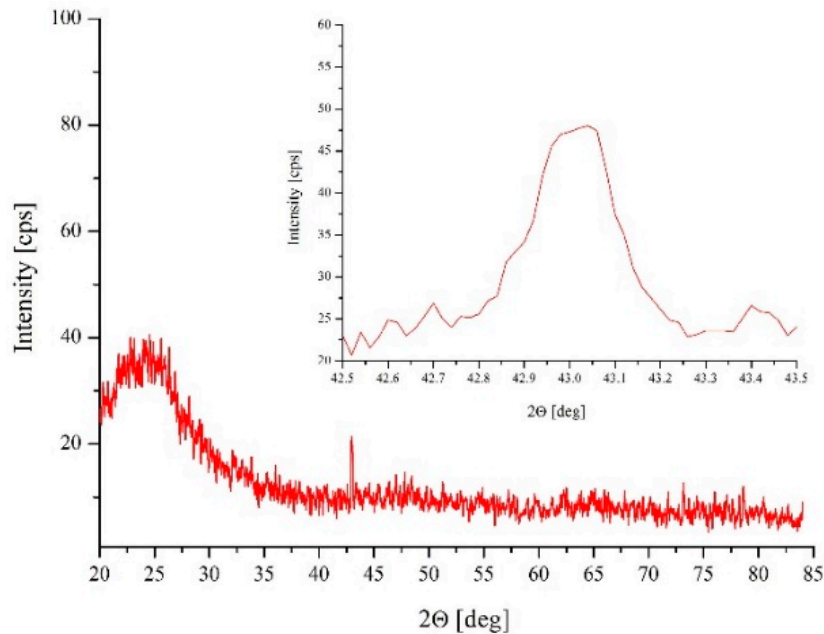


Figure 7. XRD spectra of the as-received sample.

From Figure 7, one can state that a broad peak can be found at about 22°, which belongs to the amorphous SiO₂, while a smaller peak is observable at 43° that relates to the carbon content. These results are in good agreement with the results presented in [28]. The carbon content can originate as the side effect of the preparation (super critical CO₂ extraction). In Figures 8 and 9, the XRD results of the annealed samples can be found.

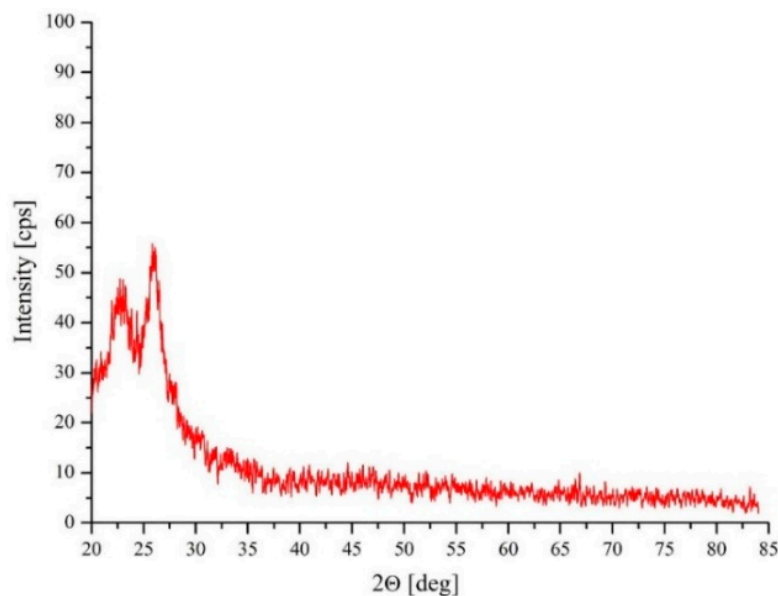


Figure 8. The X-ray diffractometer (XRD) spectra of the isothermally annealed samples.

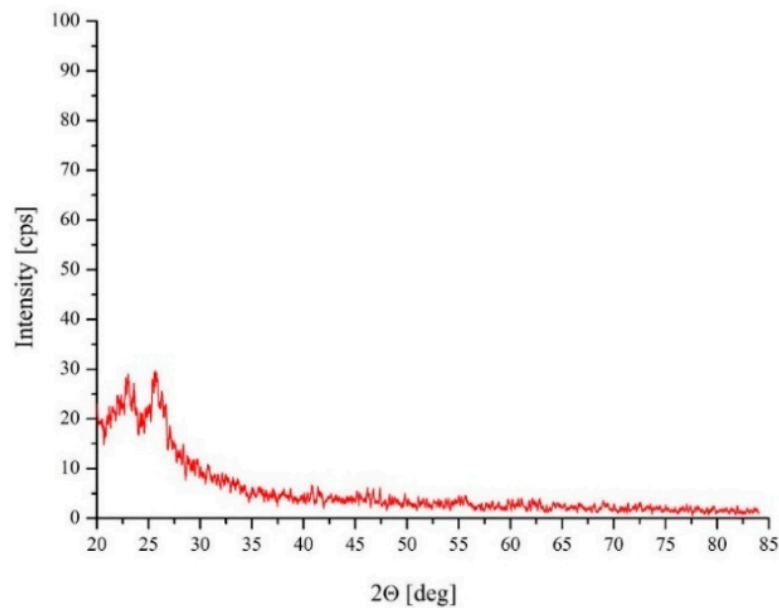


Figure 9. The X-ray diffractometer (XRD) spectra of the isochronally annealed samples.

From both graphs (Figures 8 and 9), one can see that the peak at 43° disappears as a result of annealing, while besides the broad peak observed on as-prepared sample near 22° , a new peak appears. These twin peaks were reported by Zhou et al. [28]. From these results, we could expect that heat treatment in such materials causes either a crystallization process or the growth of the grains. In Reference [45], it was stated that the different types of measurements carried out on fiber aerogel samples are very important, as they support each other. Reference [46] stated that the artificial aging of insulation materials and their investigations with different methods are very important.

4. Conclusions

Silica aerogels present acceptable thermal conductivity, and they are mainly used as thermal superinsulators. Here, we studied the influence of aging and drying processes on the microstructure and thermal properties of aerogel samples. Glass wool–silica gel composites were aged (thermal annealed) for variable temperatures and times at ambient air. Different experimental results were presented, supporting each other, and were carried out on glass fiber-reinforced aerogel samples. The tests of different laboratories supported the main conclusion of this paper. We can declare that thermal aging has an effect on the properties of the insulation materials. We observed the microstructural changes by sorption measurements through the variations of the shapes of the curves as well as by scanning electron microscopy; then, we manifested the growing of the grains. Furthermore, with X-ray diffraction, and last but not least with differential scanning calorimetry, we presented the changes in the phases and the presence of kinetic reactions. We pointed out that the aerogel grains are growing due to the thermal annealing and separating from the glass fibers. These results were combined with previously published ones, where the changes in the thermal conductivity caused by the thermal annealing were manifested. These results could provide a good base for the designers to know the applicability limit of the samples in high-temperature places.

Author Contributions: Conceptualization, Á.L.; Investigation, Á.L, A.C, I.B. and A.T.; Methodology, Á.L.; Supervision, Á.L.; Writing—original draft, Á.L., A.C., and A.T.; Writing-review & editing, Á.L., A.C. and A.T.

Funding: The research was financed the Ministry of Human Capacities in Hungary (grant number 20428-3/2018/FEKUTSTRAT).

Acknowledgments: The research was financed by the Higher Education Institutional Excellence Programme of the Ministry of Human Capacities in Hungary, within the framework of the Energetics thematic programme

of the University of Debrecen. The author A.T. gratefully acknowledges a financial support for his work from RVO: 11000.

Conflicts of Interest: The authors declare no conflict of interest.

References

1. Kalmár, F. Energy analysis of building thermal insulation. In Proceedings of the 11th Conference for Building Physics, Dresden, Germany, 26–30 September 2002; pp. 103–112.
2. Kunic, R. Carbon footprint of thermal insulation materials in building envelopes. *Energy Effic.* **2017**, *10*, 1511–1528.
3. Szabó, G.L.; Kalmár, F. Parametric analysis of buildings' heat load depending on glazing—Hungarian case study. *Energies* **2018**, *11*, 3291. [[CrossRef](#)]
4. Csáky, I.; Kalmár, F. Investigation of the relationship between the allowable transparent area, thermal mass and air change rate in buildings. *J. Build. Eng.* **2017**, *12*, 1–7. [[CrossRef](#)]
5. Iswara, S.; Griffa, M.; Kaufmann, R.; Beltrand, M.; Hubera, L.; Brunner, S.; Lattuada, M.; Koebel, M.M.; Malfait, W.J. Effect of aging on thermal conductivity of fiber-reinforced aerogel composites: An X-ray tomography study. *Microporous Mesoporous Mater.* **2019**, *278*, 289–296. [[CrossRef](#)]
6. Lakatos, Á. Stability investigations of the thermal insulating performance of aerogel blanket. *Energy Build.* **2019**, *139*, 506–516. [[CrossRef](#)]
7. Aegerter, A.; Leventis, N.; Koebel, M. *Aerogels Handbook*; Springer: New York, NY, USA, 2011; pp. 537–564.
8. Hostler, S.R.; Abramson, A.R.; Gawryla, M.D.; Bandi, S.A.; Schiraldi, D.A. Thermal conductivity of a clay-based aerogel. *Int. J. Heat Mass Transf.* **2008**, *52*, 665–669. [[CrossRef](#)]
9. Schultz, J.M.; Jensen, K.I.; Kristiansen, F.H. Super insulating aerogel glazing. *Solar Energy Mater. Solar Cells* **2005**, *89*, 275–285. [[CrossRef](#)]
10. Galliano, R.; Wakili, K.G.; Stahl, T.; Binder, B.; Daniotti, B. Performance evaluation of aerogel-based and perlite-based prototyped insulations for internal thermal retrofitting: HMT model validation by monitoring at demo scale. *Energy Build.* **2016**, *12*, 275–286. [[CrossRef](#)]
11. Wakili, K.G.; Stahl, T.; Heiduk, E.; Schuss, M.; Vonbank, R.; Pont, U.; Sustr, C.; Wolosiuk, D.; Mahdavi, D. High performance aerogel containing plaster for historic buildings with structured façades. *Energy Procedia* **2015**, *78*, 949–954. [[CrossRef](#)]
12. Lucchi, E.; Becherini, F.; Di Tuccio, M.C.; Troi, A.; Frick, J.; Roberti, F.; Hermann, C.; Fairnington, I.; Mezzasalma, G.; Pockelé, L.; et al. Thermal performance evaluation and comfort assessment of advanced aerogel as blown-in insulation for historic buildings. *Build. Environ.* **2017**, *122*, 258–268. [[CrossRef](#)]
13. Lucchi, E.; Roberti, F.; Alexandra, T. Definition of an for the thermal performance evaluation of inhomogeneous walls. *Energy Build.* **2018**, *179*, 99–111. [[CrossRef](#)]
14. Berardi, U.; Lakatos, Á. Thermal bridges of metal fasteners for aerogel-enhanced blankets. *Energy Build.* **2019**, *185*, 307–315. [[CrossRef](#)]
15. Stahl, T.; Brunner, S.; Zimmermann, M.; Wakili, K.G. Thermo-hygric properties of a newly developed aerogel based insulation rendering for both exterior and interior applications. *Energy Build.* **2012**, *44*, 114–117. [[CrossRef](#)]
16. Cuce, E.; Cuce, P.M.; Wood, C.J.; Riffat, S.B. Toward aerogel based thermal superinsulation in buildings: A comprehensive review. *Renew. Sustain. Energy Rev.* **2014**, *34*, 273–299. [[CrossRef](#)]
17. Baetens, R.; Jelle, B.P.; Gustavsen, A. Aerogel insulation for building applications: A state-of-the-art review. *Energy Build.* **2011**, *43*, 761–769. [[CrossRef](#)]
18. Lakatos, Á. Investigation of the moisture induced degradation of the thermal properties of aerogel blankets: Measurements, calculations, simulations. *Energy Build.* **2017**, *139*, 506–516. [[CrossRef](#)]
19. Hoseini, A.; Bahrami, M. Effects of humidity on thermal performance of aerogel insulation blankets. *J. Build. Eng.* **2017**, *13*, 107–115. [[CrossRef](#)]
20. Nosrati, R.H.; Berardi, U. Hygrothermal characteristics of aerogel-enhanced insulating materials under different humidity and temperature conditions. *Energy Build.* **2018**, *158*, 698–711. [[CrossRef](#)]
21. Jelle, B.P. Accelerated climate ageing of building materials, components and structures in the laboratory. *J. Mater. Sci.* **2012**, *47*, 6475–6496. [[CrossRef](#)]

22. Jelle, B.P. Traditional, state-of-the-art and future thermal building insulation materials and solutions—properties, requirements and possibilities. *Energy Build.* **2011**, *43*, 2549–2563. [[CrossRef](#)]
23. Miros, A. Thermal Aging Effect on Thermal Conductivity Properties of Mineral Wool Pipe Samples at High Temperature. In Proceedings of the 3rd World Congress on Mechanical, Chemical, and Material Engineering (MCM'17), Rome, Italy, 8–10 June 2017.
24. Yang, X.; Sun, Y.; Shi, D.; Liu, J. Experimental investigation on mechanical properties of a fiber-reinforced silica aerogel composite. *Mater. Sci. Eng. A* **2011**, *528*, 4830–4836. [[CrossRef](#)]
25. Chakraborty, S.; Pisal, A.A.; Kothari, V.K.; Rao, A.V. Synthesis and Characterization of Fibre Reinforced Silica, Aerogel Blankets for Thermal. *Adv. Mater. Sci. Eng.* **2016**, *2016*. [[CrossRef](#)]
26. Li, Z.; Gong, L.; Cheng, X.; He, S.; Li, C.; Zhang, H. Flexible silica aerogel composites strengthened with aramid fibers and their thermal behavior. *Mater. Des.* **2016**, *99*, 349–355. [[CrossRef](#)]
27. Shafi, S.; Navik, R.; Ding, X.; Zhao, Y. Improved heat insulation and mechanical properties of silica aerogel/glass fiber composite by impregnating silica gel. *J. Non-Cryst. Solid* **2019**, 503–504. [[CrossRef](#)]
28. Zhu, L.; Wang, Y.; Cui, S.; Yang, F.; Nie, Z.; Li, Q.; Wei, Q. Preparation of silica aerogels by ambient pressure drying without causing equipment corrosion. *Molecules* **2018**, *23*, 1935. [[CrossRef](#)]
29. Zhou, T.; Gong, L.; Cheng, X.; Pan, Y.; Li, C.; Zhang, H. Preparation and characterization of silica aerogels from by-product silicon tetrachloride under ambient pressure drying. *J. Non-Cryst. Solid* **2018**, *499*, 387–393. [[CrossRef](#)]
30. Hasan, M.A.; Rashmi, S.; Esther, A.C.M.; Bhavanisankar, P.Y.; Sherikar, B.; Sridhara, N.; Dey, A. Evaluations of silica aerogel-based flexible blanket as passive thermal control element for spacecraft applications. *J. Mater. Eng. Perform.* **2018**, *27*, 1265–1273. [[CrossRef](#)]
31. Lakatos, Á. Thermal conductivity of insulations approached from a new aspect. *J. Therm. Anal. Calorim.* **2018**, *133*, 329–335. [[CrossRef](#)]
32. EN ISO 12664. *Thermal Performance of Building Materials and Products. Determination of Thermal Resistance by Means of Guarded Hot Plate and Heat Flow Meter Methods*; Dry and moist products of medium and low thermal resistance, CEN–EN–Standard; BSI: London, UK, 2001.
33. ASTM C518-17. *Standard Test Method for Steady-State Thermal Transmission Properties by Means of the Heat Flow Meter Apparatus*; ASTM International: West Conshohocken, PA, USA, 2017.
34. ISO 8301. *ISO 8301:1991 Thermal Insulation Determination of Steady-State Thermal Resistance and Related Properties Heat Flow Meter Apparatus*; American National Standards Institute (ANSI): Washington, DC, USA, 1991.
35. Lakatos, Á. Method for the determination of sorption isotherms of materials demonstrated through soil samples. *Int. Rev. Appl. Sci. Eng.* **2011**, *2*, 117–121. [[CrossRef](#)]
36. Lakatos, Á.; Deák, I.; Berardi, U. Thermal characterization of different graphite polystyrene. *Int. Rev. Appl. Sci. Eng.* **2018**, *9*, 163–168. [[CrossRef](#)]
37. Lakatos, Á.; Trnik, A. Thermal characterization of fibrous aerogel blanket. *AIP Conf. Proc.* (accepted).
38. EN ISO 12571. *Hygrothermal Performance of Building Materials and Products—Determination of Hygroscopic Sorption Properties*; BSI: Dublin, Ireland, 2013.
39. DIN 51007. *General Principles of Differential Thermal Analysis*; Deutsches Institut für Normung, DIN: Berlin, Germany, 1994.
40. EN ISO 12667. *Thermal Performance of Building Materials and Products. Determination of Thermal Resistance by Means of Guarded Hot Plate and Heat Flow Meter Methods*; Products of high and medium thermal resistance; BSI: London, UK, 2001.
41. Brunauer, S.; Deming, L.S.; Deming, W.E.; Teller, E. On a theory of the van der Waals adsorption of gases. *J. Am. Chem. Soc.* **1940**, *62*, 1723–1732. [[CrossRef](#)]
42. Liang, Y.; Wu, H.; Huang, G.; Yang, J.; Wang, H. Thermal performance and service life of vacuum insulation panels with aerogel composite cores. *Energy Build.* **2017**, *154*, 606–617. [[CrossRef](#)]
43. Musić, S.; Filipović-Vinceković, N.; Sekovanić, L. Precipitation of amorphous SiO₂ particles and their properties. *Braz. J. Chem. Eng.* **2011**, *28*, 89–94. [[CrossRef](#)]
44. Kwon, Y.G.; Choi, S.E.Y. Ambient-dried silica aerogel doped with TiO₂ powder for thermal insulation. *J. Mater. Sci.* **2000**, *35*, 6075–6079. [[CrossRef](#)]

45. Zhang, H.; Zhang, C.; Ji, W.; Wang, X.; Li, Y.; Tao, W. Experimental characterization of the thermal conductivity and microstructure of opacifier-fiber-aerogel composite. *Molecules* **2018**, *23*, 2198. [[CrossRef](#)] [[PubMed](#)]
46. Kunic, R. Vacuum insulation panels—an assessment of the impact of accelerated ageing on service life. *Strojniški Vestnik—J. Mech. Eng.* **2012**, *58*, 598–606. [[CrossRef](#)]



© 2019 by the authors. Licensee MDPI, Basel, Switzerland. This article is an open access article distributed under the terms and conditions of the Creative Commons Attribution (CC BY) license (<http://creativecommons.org/licenses/by/4.0/>).